Mon. Not. R. Astron. Soc. **000**, 1–8 (2015) Printed 4 April 2015 (MN LATEX style file v2.2)

Results of two multi-chords stellar occultations by dwarf planet (1) Ceres

A. R. Gomes-Júnior[1,⋆], B. L. Giacchini[2,3,4],F. Braga-Ribas[5,6,†] M. Assafin[1,†], R. Vieira-Martins[1,5,†], J.I.B. Camargo[5,†], B. Sicardy[7], B. Timerson[4], T. George[4], J. Broughton[8], T. Blank[4], G. Benedetti-Rossi[5], J. Brooks[4], R. F. Dantowitz[9], D. W. Dunham[4], J. B. Dunham[4], C. K. Ellington[4], M. Emilio[10], F.R. Herpich[11], C. Jacques[12], P. D. Maley[4,13], L. Mehret[10], A.J.T. Mello[11], A.C. Milone[14], E. Pimentel[12], W. Schoenell[11], N. S. Weber[9]

[1] *Observatório do Valongo/UFRJ, Ladeira Pedro Antônio 43, CEP 20.080-090 Rio de Janeiro - RJ, Brazil*
[2] *Centro Brasileiro de Pesquisas Físicas, Rua Dr. Xavier Sigaud 150, Rio de Janeiro 22290-180, Brazil*
[3] *Seção de Ocultações/REA-Brasil, Av. Prof. Magalhães Penido 403/302, Belo Horizonte 31270-700, Brazil*
[4] *International Occultation Timing Association, P.O. Box 131034, Houston, TX 77219-1034, USA*
[5] *Observatório Nacional/MCT, R. General José Cristino 77, CEP 20921-400 Rio de Janeiro - RJ, Brazil*
[6] *Federal University of Technology - Paraná (UTFPR / DAFIS), Rua Sete de Setembro, 3165, CEP 80230-901, Curitiba, PR, Brazil*
[7] *LESIA, Observatoire de Paris, CNRS UMR 8109, Université Pierre et Marie Curie, Université Paris-Diderot, 5 place Jules Janssen, F-92195 Meudon Cedex, France*
[8] *RASNZ Occultation Section, 18 Branch Cr. Reedy Creek, QLD 4227, Australia*
[9] *Clay Center Observatory at Dexter Southfield, 20 Newton Street, Brookline, MA 02445, USA*
[10] *Universidade Estadual de Ponta Grossa, Ponta Grossa, Brazil*
[11] *Universidade Federal de Santa Catarina, Florianópolis, Brazil*
[12] *Centro de Estudos Astronômicos de Minas Gerais, Belo Horizonte, Brazil*
[13] *NASA Johnson Space Center Astronomical Society, 4535 Cedar Ridge Trail, Houston, TX 77059 USA*
[14] *Instituto Nacional de Pesquisas Espaciais, SÃčo JosÃľ dos Campos, Brazil*
[†] *Associated to Laboratório Interinstitucional de e-Astronomia - LIneA, Rua Gal. José Cristino 77, CEP 20921-400, Rio de Janeiro, Brazil*

Accepted . Received ; in original form

ABSTRACT

We report the results of two multi-chord stellar occultations by the dwarf planet (1) Ceres that were observed from Brazil on August 17 2010, and from USA on October 25 2013. Four positive detections were obtained for the 2010 occultation, and nine for the 2013 occultation. Elliptical models were adjusted to the observed chords to obtain the Ceres' size and shape. Two limb fitting solution were studied for each event. The first one is a nominal solution with an indeterminate polar aspect angle. The second one was constrained by the pole coordinates as given by Drummond et al. (2014). Assuming a Maclaurin spheroid, we determine an equatorial diameter of 972 ± 6 km and an apparent oblateness of 0.08 ± 0.03 as our best solution. These results are compared to all available size and shape determinations for Ceres made so far, and shall be confirmed by the Nasa's *Dawn* space mission.

Key words: minor planets, asteroids: individual (1, Ceres) - occultations - planets and satellites: fundamental parameters

1 INTRODUCTION

Ceres is the sole exemplar of a dwarf planet in the inner Solar System. Far from being a mere taxonomic information, this suggests the great impact its study can have on the understanding of planetary formation and evolution of the Solar System. Indeed, it was proposed that Ceres could have its origin as a transneptunian object (McKinnon 2012), later scattered to the Main Belt due to the giant planets' migration predicted by the 'Nice Model' (Gomes et al. 2005).

⋆ E-mail: altair08@astro.ufrj.br

It may well had been formed close to its current location, however, even on this scenario, the dynamical history of the Solar System must have let its signatures on Ceres. Not only on the late heavy bombardment features that might exist on its surface, but also on its volatiles, which could have been transported from the outer region.

Since the 1970's it has been speculated that Ceres could contain water ice, what was recently verified (Küppers et al. 2014). Although the water regime on this object is still unknown, some internal structure models suggest the existence of a water ice – or even a liquid water – layer (Castillo-Rogez 2011). Yet the very question of whether Ceres suffered differentiation is open and, on the assumption of an affirmative answer, it is natural to ask if it ever had tectonics, how its geological evolution was, and if it is still active. Inarguably NASA's *Dawn* mission (Russell et al. 2004), that is currently orbiting the dwarf planet, will shed light on several open issues concerning Ceres.

Owning approximately one fifth of the whole Main Belt's mass, Ceres is expected to have an equilibrium figure, i.e. a Maclaurin or a Jacobi ellipsoid. In fact, direct observations of Ceres by means of adaptive optics indicate that it is an oblate spheroid (Drummond et al. 2014). The precise knowledge of its size and shape is of utmost importance, for the models of density, internal structure and differentiation.

The best ground-based technique for determining shape and size of a faraway object is the study of its shadow, cast by a star during an occultation. Since the 1960's occultations have provided measurements of hundreds of asteroids, thanks partially to the fruitful professional-amateur collaboration on the field. More recently, this technique has been applied to objects of the outer Solar System and has unveiled outstanding features of distant bodies, e.g. the ring system around the Centaur (10199) Chariklo (Braga-Ribas et al. 2014).

The first stellar occultation by Ceres was observed in 1984 (Millis et al. 1987) and led to the determination of its size to the precision of some kilometres, in a time when the uncertainties were often ten times larger. The low apparent magnitude of Ceres, if compared to most asteroids, imposes a somewhat strong constraint on the stars capable of causing a detectable magnitude drop when occulted. For instance, after the 1984 event, to our knowledge, only four stellar occultations have been observed. Two of them had only two chords each, not sufficient, thus, for providing accurate results[1]. The two remaining events, which occurred on 17 August 2010 and 25 October 2013, are reported on the present work and are the first ones that used charged-couple devices (CCD) as recording systems. Throughout the paper we shall refer to these events as the '2010 occultation' and the '2013 occultation'.

Both events were predicted by Steve Preston[2] on behalf of the International Occultation Timing Association, during routine prediction of asteroidal occultations of bright stars.

This work is organized as follows. In Sections 2 and 3 we analyse, the 2010 and the 2013 occultations, respectively. In Section 4 we give the geocentric positions of Ceres derived from the occultations. The comparison of both results to those on the literature is carried out in Section 5.

[1] These events took place on 22 August 1994 and 30 October 2010.

[2] Predictions are published at http://asteroidoccultation.com.

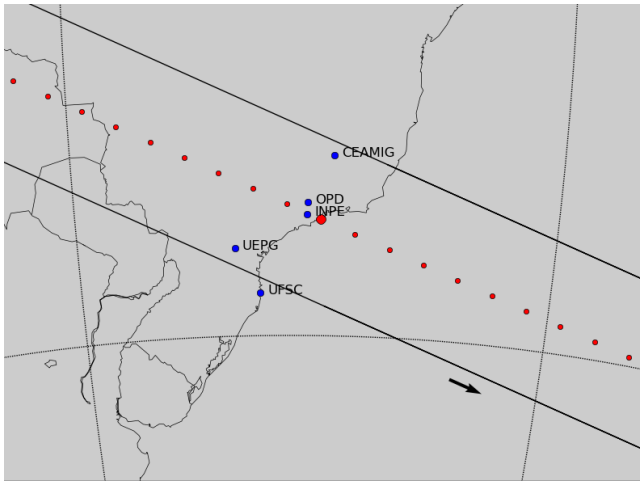

Figure 1. Post-occultation reconstruction of Ceres' shadow path on Earth for the 2010 August 17 event. The big red dot is the geocentric closest approach at 22:40:25 UT. The small red ones represent the centre of the shadow separated by one minute, shadow moves from the left to the right. Blue dots are the sites that have observed the event. As described in text, UFSC had a negative chord.

2 THE 2010 OCCULTATION

2.1 Observations

On 17 August 2010 Ceres was predicted to occult the star TYC 6833-163-1, which has magnitude $V = 11.55$ and has the ICRS position:

$$\begin{cases} \alpha = 17^{\rm h}18^{\rm m}29^{\rm s}.008 \\ \delta = -27^{\circ}26'38''.890. \end{cases} \quad (1)$$

Observations were carried out in Brazil from five different sites as displayed in Table 1 and Fig. 1. The occultation was detected on four of them. The south most one (UFSC) had a negative chord. From the positive ones, the one named INPE started the observation when the event was already in progress, thus providing only the star's reappearance time; the other three recorded the whole phenomenon.

A remarkable circumstance of this event was the low velocity of Ceres: only 3.9 $km.s^{-1}$ in the plane of the sky. Therefore, even exposures of a few seconds would translate in a relevant spatial resolution.

All the observations were made through a sequence of images obtained with CCDs. The times of each exposure were available on the header of each image with an internal accuracy of a few hundredths of a second. CEAMIG had only the integer part of the second available, due to the acquisition software used. The fraction of a second could be retrieved as described on the Section 3.1 of Braga-Ribas et al. (2013) (which shall be referred as BR13 hereafter). Cycle times (exposure plus read-out) varied from 2 to 52 seconds, as can be verified on Table 1, making of it an heterogeneous set of observations and imposing an error of a few seconds for the ingress / egress times of some sites.

Table 1. Circumstances of observation for all observing stations of the 2010 event.

Site	Longitude Latitude Height	Telescope Aperture f-ratio	Exposure Cycle time Camera	Result Ingress Egress	Observer
Belo Horizonte	43°59'51.1" W	LX200	5 s	Positive	C. Jacques
CEAMIG-REA	19°49'49.0" S	31 cm	12 s	22:39:03.9 ± 0.6	E. Pimentel
	825 m	f/10	SBIG ST10	22:40:20 ± 5	
Pico dos Dias	45°34'45.1" W	Zeiss	1 s	Positive	J. I. B. Camargo
OPD/LNA	22°32'03.7" S	60 cm	2 s	22:37:30.3 ± 0.6	G. B. Rossi
	1864 m	f/12.5	Andor Ikon	22:41:55.3 ± 0.7	
São José dos	45°51'44.0" W	C11	2 s	Egress only	A. C. Milone
Campos	23°12'33.0" S	28 cm	5 s	Start obs.: 22:39:44	T. Maldonado
INPE	975 m	f/6.3	SBIG ST7	22:42:03.0 ± 0.2	M. Okada
Ponta Grossa	50°05'56.0" W	RCX 400	30 s	Positive	M. Emilio
UEPG	25°05'22.2" S	40 cm	52 s	22:37:17 ± 13	L. Mehret
	910 m	f/8	SBIG STL6E	22:39:56 ± 13	
Florianópolis	48°31'20.5" W	C11	3 s	No occultation	W. Schoenell
UFSC	27°36'12.3" S	28 cm	6 s	Start obs.: 21:49:27	A. J. T. Mello
	20 m	f/10	SBIG ST7	End obs.: 22:51:21	F. R. Herpich

2.2 Light curves and timing

The flux of the star in the five occultation chords was obtained from the FITS images with the Platform for Reduction of Astronomical Images Automatically (PRAIA) (Assafin et al. 2011). The light curves were normalized to the flux of the star plus Ceres, as they were merged right before and after the occultation. Additionally, they were normalized by fitting a polynomial curve (of first or second order) outside the flux drop, so that the flux ratio was set to 1 outside the occultation.

The start and end times of the occultation were obtained for each light curve by fitting a square-well model convoluted with the Fresnel diffraction, the CCD bandwidth, the stellar apparent diameter, and the applied finite exposure time; see Widemann et al. (2009) and BR13. The smallest integration time used in the positive observations was 1.0 s, which translates to almost 3.9 km in the celestial plane. Therefore, the occultation light curves are largely dominated by the integration times, not by Fresnel diffraction or star diameter, which are on the order a few hundreds meters for this event. The occultation fits consist in minimizing a classical χ^2 function for each light curve, as described in Sicardy et al. (2011) and BR13. The free parameter to adjust is the ingress (disappearance) or egress (reappearance) time, which provides the minimum value of χ^2, denoted as χ^2_{min}. The best fittings to the 2010 occultation light curves are shown in Fig. 2, and the derived occultation times are listed in Table 1.

2.3 Limb fitting methodology

The methodology used to analyse Ceres' profile from the observations is the same described by Sicardy et al. (2011) and BR13. To each combination of site position and recorded ingress/egress time, together with star coordinates and Ceres' ephemeris, corresponds a point on the plane of the sky. The collection of those points ideally determines the apparent limb of Ceres.

We adopt an elliptic model for the limb profile, resulting from the projection of an oblate spheroid onto the sky plane. This model is supported by the work of Drummond et al. (2014), by means of direct imaging of Ceres. Hence, we have $N = 7$ chord extremities to adjust the $M = 5$ parameters which define an ellipse: apparent semimajor and semiminor axis (a' and b', respectively), position angle P of its semiminor axis and the position (f_c, g_c) of its centre with respect to the occulted star. Of course, the apparent semimajor axis a' is equivalent to the equatorial radius R_{equa} of the ellipsoid. The coordinates f_c and g_c, in kilometres, are calculated using the JPL#26 Ceres' ephemeris and the occulted star's position. They are positive toward the local celestial east and north, respectively. The position angle P is counted positively from the direction of local celestial north to celestial east. The apparent oblateness can be defined by $\epsilon' = 1 - (b'/a')$. We define the number of degrees of freedom of the problem as $\mathcal{N} \equiv N - M$. All the procedure that allows the determination of the error bars of the physical parameters can be found on BR13.

2.4 Limb fitting solutions

Two possible solutions were considered for the limb fitting. The first is the nominal one, which consists of determining the five parameters that characterize an ellipse from the seven observed contacts. As we shortly show, it led to a rather large uncertainty on the position angle. Furthermore, the nominal solution solely is not capable of returning the true oblateness, which can be evaluated through equation 2 of BR13.

From observations with adaptive optics spanning a 10-year period, Drummond et al. (2014) determined the posi-

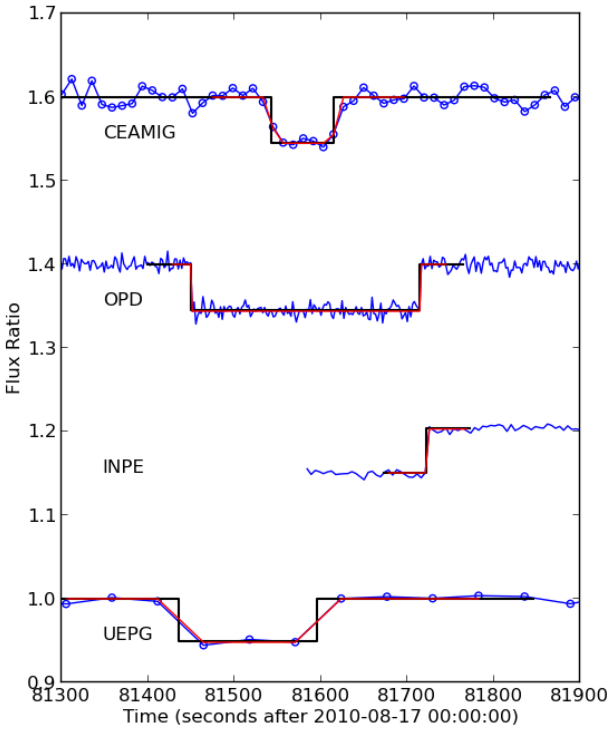

Figure 2. The four occultation light curves normalized and vertically shifted by a factor of 0.2 for better visualisation. The solid black lines are the best fit of the square-well model to the data. Red lines are the square-well model convoluted with the Fresnel diffraction, the star diameter, and the applied exposure time. The mid-times of the occultations do not coincide due to the propagation delays of the shadow due to the distinct longitude of the sites. Exposures at INPE started after the immersion, as explained in the text.

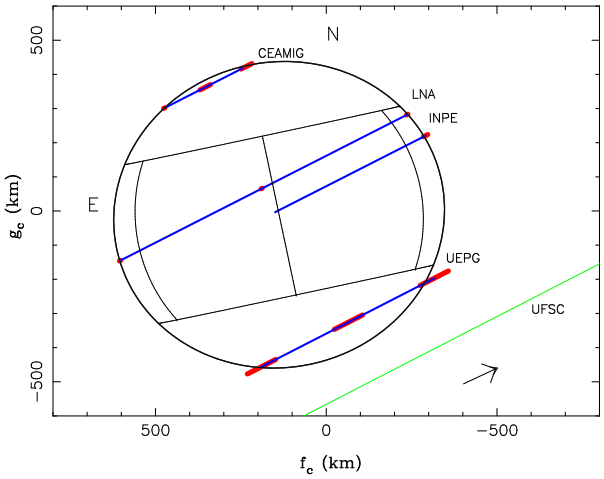

Figure 3. The best elliptical fit for the occultation chords for the event of 2010 using the times from Table 1 and the pole-constrained solution. The arrow indicates the direction of motion, blue lines are the observed chords, the red segments are the ingress, egress and mid-occultation error bars at 1-σ level.

tion of Ceres' polar axis within a range of only 3°:

$$\alpha = (287 \pm 3)^\circ, \quad \delta = (+64 \pm 3)^\circ, \tag{2}$$

in equatorial J2000 coordinates. Together with Ceres' ephemeris at the moment of the occultation, this corresponds to the polar aspect angle $\zeta = 86.1^\circ$, which is very close to an equator-on geometry. Hence, we expect true figures to be similar to apparent ones.

The knowledge of Ceres' pole not only allows the determination of its polar aspect, it suffices to set its position angle. Therefore Eq. 2 may act as a constraint for P, and a second solution can be obtained by probing the parameter space with the restriction that the position angle is confined to the range that follows from Eq. 2. We call this the "pole-constrained solution".

2.4.1 Nominal solution

With the seven observed contacts it is possible to adjust the five parameters which define an ellipse. For the best-fitting solution we find $\chi^2_{r,min} = 0.24$, which could be interpreted as a slightly overestimation of the error bars with regard to the good quality of the fit. However, inasmuch as the problem has only two degrees of freedom, it is far from the statistical realm and low $\chi^2_{r,min}$ may eventually happen.

The resulting values of equatorial diameter, oblateness, position angle and centre coordinates are presented in the second column of Table 2.

Already mentioned, the parameter with the largest uncertainty is the position angle: spanning on a 20° interval, its determination has a relative precision worse than 10%. Clearly, the coordinates of Ceres' pole (Eq. 2) can impose a strong constraint on the position angle, as the next solution shows.

Finally, the correction to the oblateness due to Ceres' polar aspect angle lies within the 1-sigma error bar and has no statistical relevance; hence $\epsilon = 0.08 \pm 0.03$.

2.4.2 Pole-constrained solution

At the moment of the occultation, the coordinates (Eq. 2) of Ceres' rotational pole correspond to the position angle $P = (12 \pm 3)^\circ$. Exploration of the parameter space, restricted to ellipses whose position angle lies on this range, results in the pole-constrained solution. The related physical parameters are displayed on the third column of Table 2 in boldface, while the best-fitting solution is depicted in Fig.3.

We notice that the constraint corresponds to the upper limit of nominal solution's 1-sigma error bar for P. On the other hand, it selects the smallest values of semimajor axis, improving its determination by a factor of about 2. Notwithstanding, oblateness' figures remain the same.

Table 2. Results of limb fitting to the data of the 2010 and 2013 events.

Solution	2010/Nominal	**2010/Pole-constrained**	2013/Nominal	2013/Pole-constrained
Equatorial diameter (km)	982 ± 14	**972 ± 6**	971 ± 7	971 ± 7
True oblateness	0.08 ± 0.03	**0.08 ± 0.03**	0.08 ± 0.04	0.08 ± 0.04
Position angle (deg)	5 ± 10	**12 ± 3** (*)	22 ± 5	25 ± 3 (*)
f_c (km)	133 ± 9	**138 ± 5**	77 ± 6	78 ± 6
g_c (km)	-17 ± 15	**-11 ± 11**	13 ± 16	13 ± 16
$\chi^2_{r,min}$	0.24	**0.42**	1.27	1.27

Notes. In bold we highlight our best solution. Error bars are at 1-sigma level. The polar diameter (D_{pol}) can be easily calculated from $D_{pol} = D_{equa}(1-\epsilon)$. (*) Position angle derived from Ceres' rotational pole coordinates determined by Drummond et al. (2014).

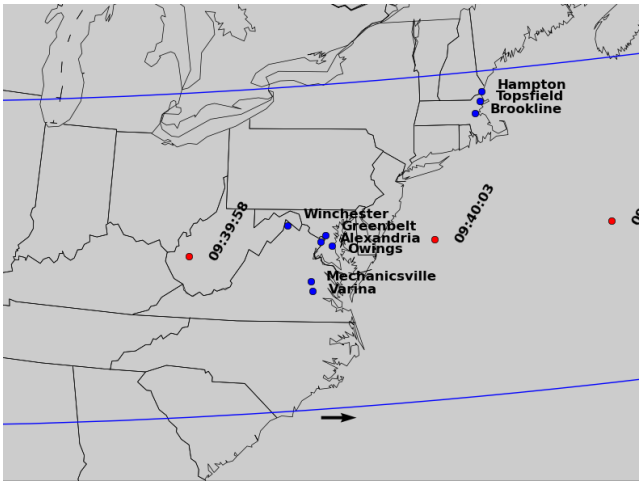

Figure 4. Post-occultation reconstruction of Ceres' shadow path on Earth for the 2013 October 25 event at the east coast of USA. Right Panel: Upper view of the occultation over the sites that observed the event (blue dots). Red points are the centre of the shadow separated by 5 seconds.

3 THE 2013 OCCULTATION

3.1 Observations

The event which took place on 25 October 2013 involved the star TYC 865-911-1 (UCAC4 496-058191), of magnitude $V = 10.05$. Based on UCAC4 (Zacharias et al. 2013), the ICRS position to the date of occultation corrected of proper motion is:

$$\begin{cases} \alpha = 11^h57^m52^s.7641 \\ \delta = +09^\circ07'49''.835 \end{cases} \quad (3)$$

The occultation could only be visible in the United States, before dawn.

Nine positive chords were obtained by the variety of equipment listed in Table 3. Each station was equipped with a video camera (whose readout time can be considered negligible). This is of particular importance in this event, since Ceres' shadow had the much faster speed of 42.6 km s^{-1}, if compared to the 2010 event. All the observing sites are in the United States, as depicted in Fig. 4.

Three different timing synchronization procedures were adopted among the set of observing stations. At Greenbelt and Owings the 1PPS signal of a GPS unit was used to calibrate time stamps which were inserted at each frame of the video. Time extraction is thus straightforward, after taking camera delays into account. On the other hand, at Brookline the clock would be synchronized by an internet server. A lack of connection, however, resulted in spurious times. In fact, comparison between the times obtained at this station and the others suggests that the former have a delay of about 64 s. Therefore, we do not use Brookline's times in the analysis that follows. Finally, at the remaining six stations the videos were recorded by camcorders on digital tapes. The timing method consisted in the comparison of the camcorder internal clock to a 1PPS GPS signal, before and after the recording of the occultation. Absolute timing errors of this procedure are expected to be inferior to 0.1 s.

A remarkable observing circumstance of this event is the low altitude of Ceres with respect to the horizon. Precisely, its altitude at moment of the occultation ranged between 20° (Hampton) and 15° (Winchester). Strong scintillation is expected in such a scenario which, combined to short integration times and the low magnitude drop of the event, resulted in rather noisy light curves and thus larger uncertainty in the time of the contacts, as it is shown in the next section.

3.2 Light curves and timing

All videos were converted to FITS images and the photometry of the target was obtained via PRAIA (Assafin et al. 2011). The light curves were normalized to the flux of a reference star when such was available on the field.

To reduce the noise, the data were binned by groups of five images – with the exception of Greenbelt, which was averaged in sets of ten. This procedure enlarges the effective integration times reported in Table 3 by a factor of 5 (or 10). As in the 2010 event, an additional normalization by a polynomial curve was applied.

The start and end times of the occultation were obtained by the same procedure explained in Section 2.2, Since the typical effective integration time used (0.17 s) translates to about 7 km in the celestial plane, and the Fresnel scale and star diameter are again on the order of few hundreds of meters, the theoretical occultation light curves are largely dominated by the integration times, as for the 2010 event.

The best-fittings to the occultation light curves are shown in Fig. 5, and the derived occultation times are listed in Table 3.

Table 3. Circumstances of observation for the observing stations of the 2013 event.

Site	Longitude Latitude Height	Telescope: Aperture f-ratio	Camera Cycle time	Result Ingress Egress	Observer
Hampton	70°48'59.7" W 42°53'52.8" N 7 m	12 cm f/5	PC164C-EX2 0.033 s	Positive 09:40:46.9 ± 0.1 09:40:57.26 ± 0.08	T. Blank
Topsfield	70°55'16.6" W 42°37'55.9" N 45 m	12 cm f/5	PC164C-EX2 0.033 s	Positive 09:40:45.4 ± 0.1 09:40:58.0 ± 0.1	T. Blank
Brookline	71°08'14.5" W 42°18'27.4" N 109 m	64 cm f/9.6	Infinity2-1R 0.015 s	Positive 09:41:48.00 ± 0.01 09:42:02.93 ± 0.01	N. Weber R. Dantowitz
Winchester	78°14'39.6" W 39°16'21.5" N 211 m	36 cm f/5	PC164C 0.033 s	Positive 09:40:33.26 ± 0.08 09:40:55.86 ± 0.09	J. Brooks
Greenbelt	76°52'09.4" W 38°59'12.1" N 52 m	12 cm f/2.5	PC164C-EX2 0.033 s	Positive 09:40:33.6 ± 0.1 09:40:56.4 ± 0.1	J. Dunham D. Dunham
Alexandria	77°02'28.3" W 38°49'19.1" N 8 m	7 cm f/10	Watec120N 0.067 s	Positive 09:40:33.3 ± 0.1 09:40:56.1 ± 0.1	P. Maley
Owings	76°38'06.3" W 38°41'26.5" N 38 m	25 cm f/3.3	PC164C 0.033 s	Positive 09:40:34.27 ± 0.05 09:40:56.0 ± 0.2	C. Ellington
Mechanicsville	77°23'06.7" W 37°41'26.1" N 60 m	12 cm f/2.5	PC164C-EX2 0.033 s	Positive 09:40:33.0 ± 0.1 09:40:54.8 ± 0.1	D. Dunham
Varina	77°19'49.3" W 37°25'58.6" N 19 m	12 cm f/2.5	PC164C-EX2 0.033 s	Positive 09:40:32.4 ± 0.3 09:40:53.1 ± 0.2	D. Dunham

3.3 Limb fitting solutions

Elliptic limb profiles were adjusted to all the available[3] chords by the same procedure described in Section 2.3[4]. This yielded $\chi^2_{r,min} = 13$, suggesting that an elliptic model is not satisfactory to the data. Indeed, a quick glance at a plot of the observed chords, such as in Fig. 6, shows that the Varina chord seems to be somewhat advanced with respect to the others. Taking into account that in this station time stamps were not inserted on the video frames, it is always possible to attribute this advance to an eventual problem on the correspondence between camcorder's and GPS' times. This could be caused, for example, if the camcorder delayed to start the recording and, since this was an unattended pre-pointed station, this fact would not be noticed by the analysis of the video itself.

The immersion recorded at Owings also seems to be shifted (delayed) with respect to the nearby chords (see Fig. 6). This chord, actually, has roughly the same length of Mechanicsville's, despite the fact that they are separated by about 100 *km*. Differently from Varina, though, this station had time stamps inserted in each frame of the video, which makes it more unlike to justify an eventual timing issue. Another possible explanation for the apparent problem of the times of this chord is the determination of the events in the light curve analysis, which could have been affected by noise. Finally, the delay during the ingress could be caused by a relief feature in Ceres; we shall soon return to this hypothesis.

In a second limb fitting, thus, we did not consider Brookline, Varina and Owings chords. The adjust of the five parameters which define an ellipse to the 12 contacts then resulted in $\chi^2_{r,min} = 1.27$, indicating that the fitting is in good agreement with the observed data within the error bars. This is the solution depicted in Fig. 6, where we see that the chord length measured in Brookline is compatible to the model. The associated physical parameters are presented in Table 2 as the nominal solution.

For this event the polar aspect angle is $\zeta = 90.7°$, which

[3] Brookline's chord was not used for limb fitting since it had an inaccurate absolute time.
[4] For this event, the JPL#33 Ceres' ephemeris was used to obtain the f_c and g_c coordinates.

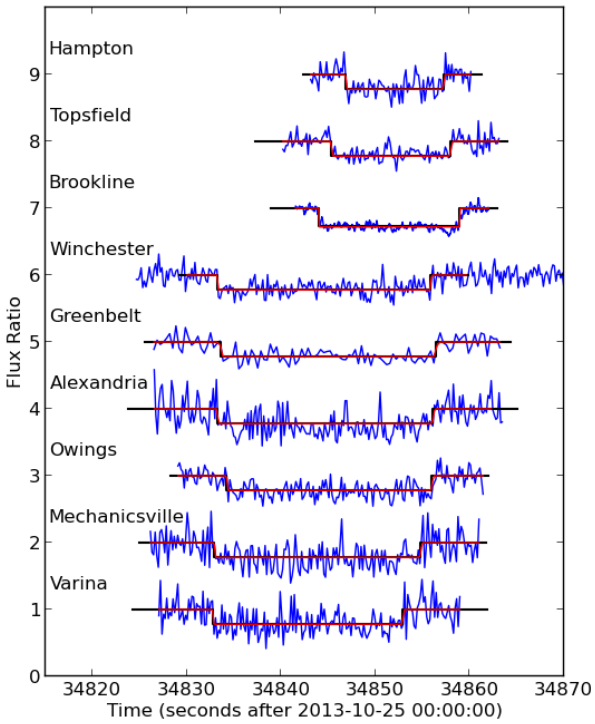

Figure 5. The nine occultation light curves normalized and vertically shifted by a factor of 1.0 for better viewing, see Fig. 2 for the explanation of the graph.The light curve of Brookline is shifted by -64 s as explained in the text.

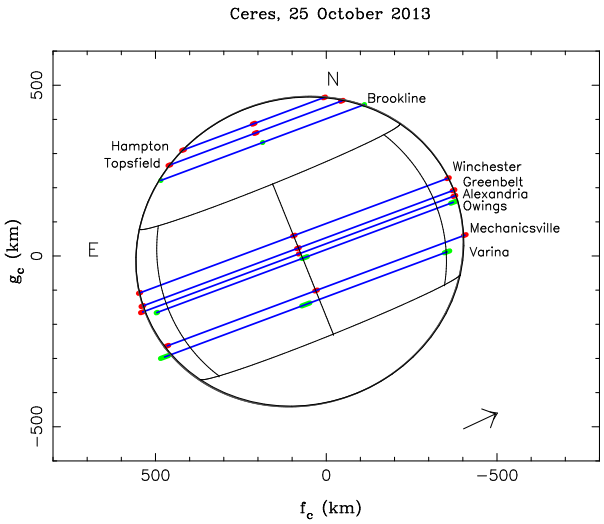

Figure 6. The best elliptical fit for the occultation chords for the event of 2013 using timing from Table 3 and the nominal solution. The arrow indicates the direction of motion, blue lines are the observed chords, the red and green segments are the ingress, egress and mid-occultation error bars at 1-σ level. The chords with green error bars were not used during the limb fit process. The chord of Brookline if shifted by -64s as explained in the text.

makes true oblateness be equal to the apparent one, within the error bars.

It is worth noting that the position angle of this nominal solution is better constrained than the respective of the 2010 occultation. Actually, the uncertainty of the former is of 5° in contrast to 10° of the latter. This suggests that the pole-constrained solution obtained via the position of Ceres' pole (Eq. 2) would not be significantly different of the nominal one.

This assumption is confirmed when we carry out the limb fitting with the constraint $P = (25 \pm 3)^\circ$, the position angle at the moment of the occultation which follows from (Eq. 2). The physical parameters related to this pole-constrained solution are presented in the last column of Table 2, and are essentially the same of the nominal solution.

We close this section returning to the hypothesis that the delay observed in the immersion at Owings could be associated to a limb topography feature. The recorded contact would then correspond to a negative elevation of 31 ± 4 km with respect to the best-fitting ellipse. Theoretical models, however, predict that relief in Ceres should be no higher than about 10–20 km (Johnson & McGetchin 1973), while published observational data sets the bound of 18 km (Carry et al. 2008). More recently, images by the probe *Dawn* also reveal an even smoother surface. The association of Owings first contact to a relief must, therefore, be ruled out.

4 ASTROMETRY FROM OCCULTATIONS

Derive geocentric position of an object from a stellar occultation was proved to be a very precious source for orbit fit proposes (Desmars et al. 2015). Usually the astrometric position is limited to the accuracy of the occulted star position, not by the limb fit. The geocentric J2000 positions of Ceres at the time of each occultation are displayed in Eqs. 4 and 5, the error on the star position were not taken into account.

$$2010\ Aug\ 17 \begin{cases} Time = 22:40:00 \\ \alpha = 17^{\rm h}18^{\rm m}29^{\rm s}.0122 \pm 0''.003 \\ \delta = -27^\circ 26' 38''.617 \pm 0''.007 \end{cases} \quad (4)$$

$$2013\ Oct\ 25 \begin{cases} Time = 09:45:00 \\ \alpha = 11^{h}57^{m}52^{s}.9154 \pm 0''.002 \\ \delta = +09^\circ 07' 49''.865 \pm 0''.007 \end{cases} \quad (5)$$

5 DISCUSSION

A quick glance at Table 2 shows there is an overall agreement between the physical parameters derived from both occultations, specially in the equatorial diameter. The differences of the solutions occur basically on the size of their error bars, and can be justified by the particularities of each set of data, as discussed below.

The 2010 event, for example, had only seven contacts; none the less, they were well distributed over Ceres' disc (see Fig. 3) acting as a constraint to is shape. On the other hand, the 2013 event had five more exploitable contacts, but they were concentrated in certain regions of the body. In particular, the absence of chords closer to Ceres' southern

Table 4. Ceres' equatorial diameter and oblateness

Eq. diameter (km)	Oblateness	Method	Ref.
972 ± 6	0.08 ± 0.03	Occultation	1
967 ± 10	0.078 ± 0.015	Keck+VTL	2
959 ± 5	0.074 ± 0.007	Keck	3
975 ± 4	0.068 ± 0.005	HST	4
959 ± 7	0.05 ± 0.01	Occultation	5

References. 1: Present work. 2: Drummond et al. (2014). 3: Carry et al. (2008). 4: Thomas et al. (2005). 5: Millis et al. (1987).

limb made its oblateness be worse determined here than in the 2010 event.

However, even our best measurement for the oblateness, $\epsilon = 0.08 \pm 0.03$, has still a higher uncertainty with regard to other figures published in the literature, as Table 4 shows. A larger number of uniformly spaced chords would be necessary to offer a best constraint to the oblateness.

The few chords of the 2010 occultation could themselves only constraint the position angle of the object to a 20° interval. This range was reduced by a factor of two in the 2013 event, approaching –and verifying– the result predicted by the work of Drummond et al. (2014). As it was shown, using the coordinates of Ceres' polar axis to limit the position angle, was not an efficient procedure in the case of this occultation, in the sense that the aforementioned limitation had not correspond to a stronger constraint on the other parameters.

On the other hand, constrain the position angle on the 2010 occultation was proved to reduce the error bars of the other parameters (disregarding oblateness). Moreover, this procedure resulted in an excellent agreement between the equatorial radius figures of both events.

The 2013 occultation, therefore, offers not only an independent verification of the figures resulted from the 2010 event, but also validates the procedure carried out there – and which led to the best-constrained parameters in this work.

Comparison of Ceres' equatorial diameter as measured by different techniques is carried out in Table 4. We note an overall agreement between our result to those obtained via direct imaging by the Hubble Space Telescope (HST) (Thomas et al. 2005), the Keck Observatory and the ESO VLT (Drummond et al. 2014). The smaller figure reported by Carry et al. (2008) may be justified by the fact that in this study the effects of limb-darking were not taken into account, as pointed out by Drummond et al. (2014).

As mentioned in the Introduction, the 1984 event (Millis et al. 1987) is the only occultation data to which we can compare our result; and it is interesting to notice that the diameters measured in each case do not agree, being our result larger than the other. It is difficult to state with sure the reasons for this divergence since we had no access to the original 1987 data or reduction methodology. We note, however, that in this occultation a variation of 0.5 s in the contact times correspond to almost 7 km on Ceres' limb, which is on the same order of the residuals of their elliptical fit. Therefore, in order to properly compare their result to ours it would be necessary to reduce their light curves with the same methodology used in the present work.

As mentioned, NASA's *Dawn* mission shall bring some light to these questions, what will be important not only for the knowledge of Ceres it self, but also for all the techniques used so far to study the physical properties of small Solar System objects, such as the stellar occultations.

ACKNOWLEDGEMENTS

ARGJ thanks the financial support of CAPES. BLG thanks CNPq. F.B.R. acknowledges PAPDRJ-FAPERJ/CAPES E-43/2013 number 144997, E-26/101.375/2014 and CDFB-CAPES/Brazil. We also acknowledge Steve Preston for the predictions of the occultations.

REFERENCES

Assafin M. et al., 2011, Gaia follow-up network for the solar system objects : Gaia FUN-SSO workshop proceedings, held at IMCCE -Paris Observatory, France, November 29 - December 1, 2010. ISBN 2-910015-63-7
Braga-Ribas F. et al., 2013, ApJ, 773, 26
Braga-Ribas F. et al., 2014, Nature, 508, 72
Castillo-Rogez, J. C. 2011, Icarus, 215, 599
Desmars, J. et al., 2015, A&A, submitted
Drummond J.D. et al., 2014, Icarus, 236, 28
Carry B. et al., 2008, A&A, 478, 235
Gomes, R., Levison, H. F., Tsiganis, K., & Morbidelli, A. 2005, Nature, 435, 466
A&A, 355, L27
Johnson T.V., McGetchin T.R., 1973, Icarus, 18, 612
Küppers M. et al., 2014, Nature, 505, 525
McKinnon, W. B. 2012, LPI Contributions, 1667, 6475
Millis R.L. et al., 1987, Icarus, 72, 507
Russell, C. T., Coradini, A., Christensen, U., et al. 2004, P&SS, 52, 465
Sicardy B. et al., 2011, Nature, 478, 493
Thomas P.C. et al., 2005, Nature, 437, 224
PASP, 111, 1515
Widemann T. et al., 2009, Icarus, 199, 458
AJ, 127, 3043
Zacharias N. et al., 2013, AJ, 145, 44